THE JOURNAL OF PHYSICAL CHEMISTRY Letters

pubs.acs.org/JPCL Letter

Band Alignment in Two-Dimensional Halide Perovskite Heterostructures: Type I or Type II?

Linghai Zhang, Xu Zhang, and Gang Lu*

Cite This: J. Phys. Chem. Lett. 2020, 11, 2910–2916 Read Online

ACCESS | Metrics & More | Article Recommendations | Supporting Information

ABSTRACT: Formation of heterostructures is often inevitable in two-dimensional (2D) halide perovskites and band alignment in 2D perovskite heterostructures is of central importance to their applications. However, controversies abound in literature on the band alignment of the 2D perovskite heterostructures. While external factors have been sought to reconcile the controversies, we show that the 2D perovskite heterostructures are in fact intrinsically prone to band "misalignment", driven by thermal fluctuations. Owing to the "softness" of inorganic layers in the perovskites, electron−phonon coupling at room temperature could be strong enough to override band offsets at zero temperature, leading to oscillatory band alignment between type-I and type-II at 300 K. We further demonstrate that by tuning the inorganic layers, one can increase the band offsets and stabilize the band alignment, paving the way for optoelectronic applications of the 2D perovskite heterostructures.

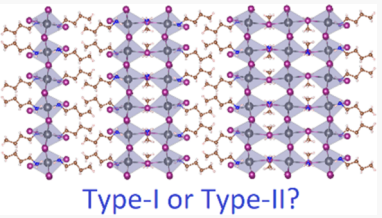

Hybrid organic−inorganic halide perovskites have emerged as some of the most promising materials for optoelectronic applications, ranging from photovoltaics to photodetectors, light-emitting diodes and lasers, etc., owing to their low fabrication costs and superior photophysical properties.[1−11] However, three-dimensional (3D) halide perovskites exhibit poor stability toward moisture and ultraviolet light, which significantly hinders their applications. In contrast, 2D and layered quasi-2D halide perovskites have shown superior stability and water resistance relative to their 3D counterparts.[12−21]

The structure of the 2D halide perovskites can be characterized as either the Ruddlesden−Popper (RP) phase with a chemical formula of $A'_2A_{n-1}M_nX_{3n+1}$ or the Dion−Jacobson (DJ) phase with a chemical formula of $A'A_{n-1}M_nX_{3n+1}$.[22−28] In the formulas, A represents a charge +1 cation, such as methylammonium (MA, $CH_3NH_3^+$) while A′ is a spacer cation. In the RP phase, A′ is a charge +1 cation, such as butylammonium (BA, $C_4H_9NH_3^+$), and in the DJ phase, A′ is a charge +2 cation, such as propanediamine (PDA, $NH_3C_3H_6NH_3^{2+}$).[29,30] M is a divalent metal cation, such as Pb^{2+} whereas X is a halide anion, such as I^-. The 2D perovskites comprise inorganic metal−halide layers separated by organic spacers and can be considered as multiple quantum wells (QWs), with the inorganic layers acting as "wells" and the organic spacers as "barriers". The positive integer n indicates the number of the inorganic layers sandwiched between the organic spacers and n can be tuned to control the width of the QWs. As a result, the 2D (n = 1) and quasi-2D (n > 1) perovskites can offer much broader structural versatility and optoelectronic tunability than either their 3D (n = ∞) counterparts or traditional quantum dots.[31−36]

However, even if a 2D perovskite film is intended to be prepared as a single phase, more often than not, it actually comprises multiple phases (with various n values from 1, 2, 3, and 4 to near ∞).[37] In other words, 2D perovskite heterostructures are unavoidable in devices. Given this inevitability and the importance of semiconductor heterojunctions in optoelectronic applications, significant research effort has been devoted to the 2D perovskite heterostructures.[37−39] Crucial to these applications is energy band alignment of the heterostructures, and two types of band alignment have been reported in the 2D perovskite heterostructures. In the type-I band alignment, the exciton (with Coulombically bonded electron and hole) funnels from a larger bandgap (smaller n) phase to a smaller bandgap (larger n) phase, resulting in energy transfer across the heterojunction. In the type-II band alignment, the electron and the hole transfer in opposite directions, leading to charge separation across the heterojunction. While the type-I alignment underlies the application of light-emitting devices, the type-II alignment is necessary for solar cells.[37,40] Therefore, determination of the band alignment, i.e., type-I vs type-II, is of paramount importance for the 2D perovskite heterostructures. Unfortunately, a definitive determination of the band alignment remains a challenge, and controversies abound in literature on the band alignment in the same 2D heterostructures.[37,40−46]

Received: February 4, 2020
Accepted: March 27, 2020
Published: March 27, 2020

https://dx.doi.org/10.1021/acs.jpclett.0c00376
J. Phys. Chem. Lett. 2020, 11, 2910–2916

For example, Pullerits et al. reported that the multilayer 2D heterostructures $(BA)_2(MA)_{n-1}Pb_nI_{3n+1}$ are of the type-I alignment,[41] while Jin et al. found them to be of the type-II alignment.[42] Similarly, the band alignment in 2D perovskite heterostructures $(PEA)_2(MA)_{n-1}Pb_nI_{3n+1}$ (PEA = $C_6H_5(CH_2)_2NH_3^+$) was reported to be type-I in some experiments[43,44] and type-II in others.[37,45]

A number of external factors have been sought to reconcile the contradictions, including film inhomogeneity, chemical treatment of the film, and difficulties in interpreting ultraviolet photoelectron spectroscopy data, etc.[47−49] More recently, De Angelis, Sargent, and co-workers have shown that the density of ligands at the heterojunctions can change the effective work-functions of the perovskites, thus resulting in different band alignments.[49] In this paper, we propose that there is an intrinsic and fundamental reason why different band alignments could arise in the same 2D heterostructure. By means of first-principles calculations, we show that owing to the "softness" of the inorganic layers, thermal fluctuations could lead to strong electron−phonon coupling in the perovskite heterostructure, resulting in significant shifts of its frontier energy levels. The energy shifts are sufficient to switch the band alignments, especially for heterostructures composed of the same inorganic layers, which is the case in those controversial experiments.[37,40−46] We reveal that the 2D perovskite heterostructures are in general prone to the band "misalignment", irrespective of the organic spacers (MA, BA, or PDA). However, the band "misalignment" can be mitigated or eliminated by tuning the inorganic layers. Our work provides a simple and consistent explanation to the contradictory experiments without seeking for extrinsic reasons. More importantly, it points to directions in which the 2D heterostructures may be engineered for more robust band alignments.

In this work, we carry out first-principles calculations based on density functional theory (DFT), time-dependent density functional theory (TDDFT), and first-principle Born−Oppenheimer molecular dynamics (BOMD) simulations for 2D perovskite heterostructures. We start with one of the simplest 2D perovskite heterostructures in the RP phase, $MA_2PbI_4/MA_3Pb_2I_7$, whose molecular structure is shown in Figure 1a. The heterostructure consists of a monolayer 2D perovskite, MA_2PbI_4 (n = 1) and a monolayer quasi-2D perovskite, $MA_3Pb_2I_7$ (n = 2), with MA cations as the organic spacer.[29] For brevity, we will use its n value to denote the 2D perovskite in the following. A number of stacking structures have been examined for the heterostructure and the most stable one is selected for band structure calculations. The computational details and molecular structures of the heterostructures are included in the Supporting Information (Figure S3, Figure S4, and Table S1).

The band structure of the 2D heterostructure at zero temperature (0 K) is computed on the basis of DFT with a range-separated hybrid functional (DFT-RSH).[50−52] The lowest-unoccupied-molecular-orbital (LUMO) and the highest-occupied-molecular-orbital (HOMO) of MA_2PbI_4 (n = 1) and $MA_3Pb_2I_7$ (n = 2) are displayed in Figure 1b. The frontier orbitals are mainly contributed by the inorganic layers of PbI_4^{2-} and $Pb_2I_7^{3-}$, respectively, with negligible contribution from MA cations. The valence band maximum (VBM) and conduction band minimum (CBM) of the heterostructure originate from the HOMO of $MA_3Pb_2I_7$ and the LUMO of MA_2PbI_4, respectively, indicating the type-II band alignment at

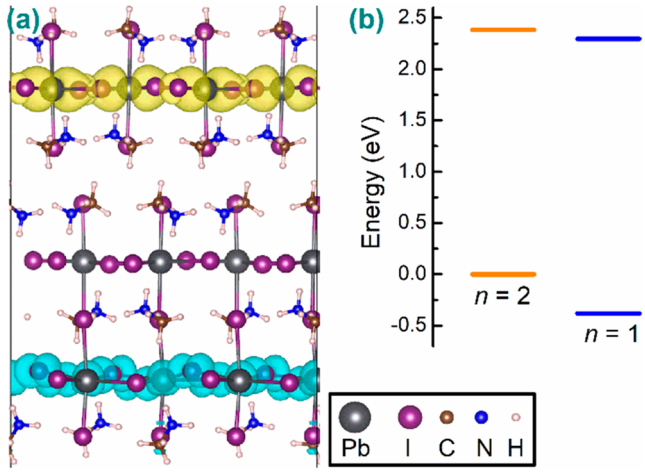

Figure 1. (a) Equilibrium molecular structure of the $MA_2PbI_4/MA_3Pb_2I_7$ heterostructure and charge density of the lowest-energy exciton with electron and hole shown in yellow and cyan, respectively. (b) Type-II band alignment of $MA_2PbI_4/MA_3Pb_2I_7$ heterostructure. The VBM of the heterostructure is set to zero.

0 K. The energy difference between the LUMOs (or the conduction band offset) is 0.09 eV, while the energy difference between the HOMOs (or the valence band offset) is 0.38 eV. Owing to large exciton binding energies in 2D perovskites,[53−56] it would be interesting to examine whether charge separation can actually take place across the interface given the type-II band alignment. To this end, we perform TDDFT calculations with the range-separated hybrid functional (TDDFT-RSH) for the lowest-energy exciton of the heterostructure at 0 K. As shown in the Figure 1a, we find that the photoexcited electron and hole are separated across the interface with the electron confined in the inorganic layer of MA_2PbI_4 and the hole in the (bottom) inorganic layer of $MA_3Pb_2I_7$. However, the exciton binding energy is estimated as 0.48 eV, much higher than the room temperature. Therefore, we conclude that the $MA_2PbI_4/MA_3Pb_2I_7$ heterojunction would not yield efficient charge separation.

Next, we set out to examine whether and how thermal fluctuations at room temperature may change the band structure of the 2D heterostructure. To this end, we carry out BOMD simulations for the $MA_2PbI_4/MA_3Pb_2I_7$ heterostructure at 300 K. In Figure 2a, we display the time evolution of the CBM and VBM of the heterostructure. The CBM and VBM can be localized entirely in MA_2PbI_4 (blue), in $MA_3Pb_2I_7$ (red), or in both of them (green). As shown in Figure 2a, significant energy fluctuation (∼0.5 eV) is observed for both CBM and VBM, more than 1 order of magnitude of the room temperature (0.025 eV). More importantly, the energy fluctuation exceeds the band offsets (0.09 and 0.38 eV) at 0 K. As a result, both the type-I and type-II band alignments could arise for the same heterostructure at 300 K. In fact, four different energy alignments, two type-I and two type-II, emerge in the heterostructure, as shown schematically in Figure 2b. The percentage of each band alignment (I_a, I_b, II_a, and II_b) is found to be 29.5%, 0.8%, 62.0%, and 7.7%, respectively, during 5 ps simulation time (Table 1). In other words, the type-I and type-II band alignment could coexist in the 2D heterostructure, with one-third probability in type-I and two-thirds probability in type-II. In Figure 3, we display the charge density of the lowest-energy exciton in the heterostructure at four different

https://dx.doi.org/10.1021/acs.jpclett.0c00376
J. Phys. Chem. Lett. 2020, 11, 2910−2916

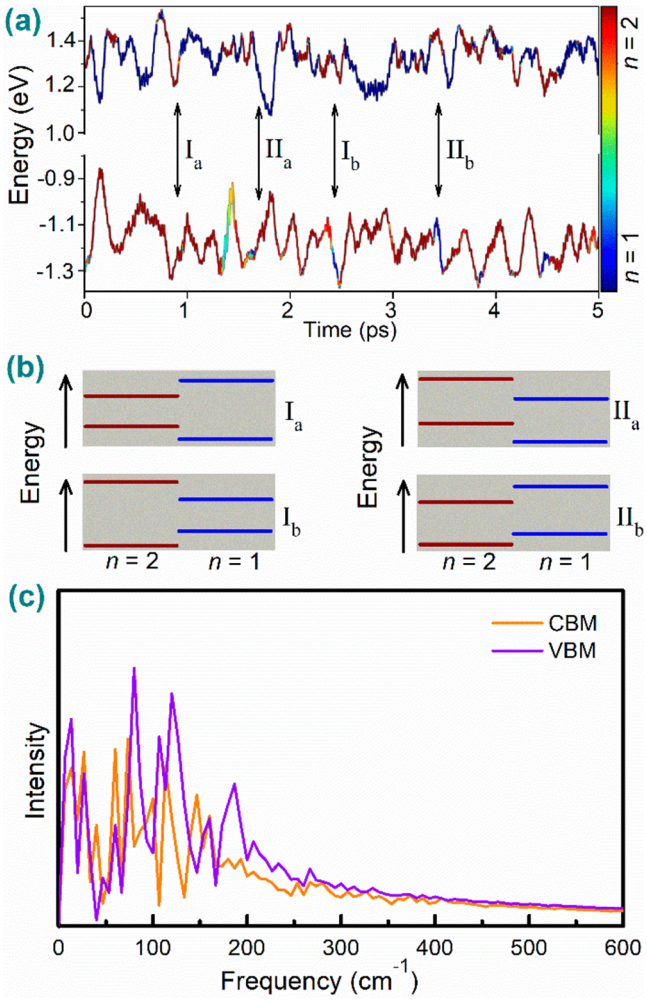

Figure 2. (a) Time evolution of CBM and VBM in $MA_2PbI_4/MA_3Pb_2I_7$ heterostructure during the BOMD simulations. (b) Schematic diagrams for the four different energy alignments (I_a, I_b, II_a, and II_b) appeared in the BOMD simulations. (c) Fourier transform of (a) from the time domain to the frequency domain.

Table 1. Percentage of the Type-I and Type-II Band Alignment in the Heterostructures of $MA_2PbI_4/MA_3Pb_2I_7$ and $MA_2PbBr_4/MA_3Pb_2I_7$ during BOMD Simulations[a]

	type-I		type-II	
	I_a	I_b	II_a	II_b
$MA_2PbI_4/MA_3Pb_2I_7$	29.5%	0.8%	62.0%	7.7%
$MA_2PbBr_4/MA_3Pb_2I_7$	17.6%	0.0%	82.4%	0.0%

[a]The percentage of I_a, I_b, II_a, and II_a is determined directly from Figures 2a and 5c, respectively.

time snapshots. The four charge density distributions are consistent with the four energy alignments identified, with entangled electron and hole corresponding to the type-I alignment and separated electron and hole corresponding to the type-II alignment. Note that our calculations are performed on atomically thin perovskites, which may undergo greater structural deformation and energy shifts than thicker ones. To model a thicker heterostructure without increasing computational effort, we fix the two MAI-terminated surface layers of the heterostructure during the BOMD simulations and re-examine the band alignment at 300 K. We find that the results

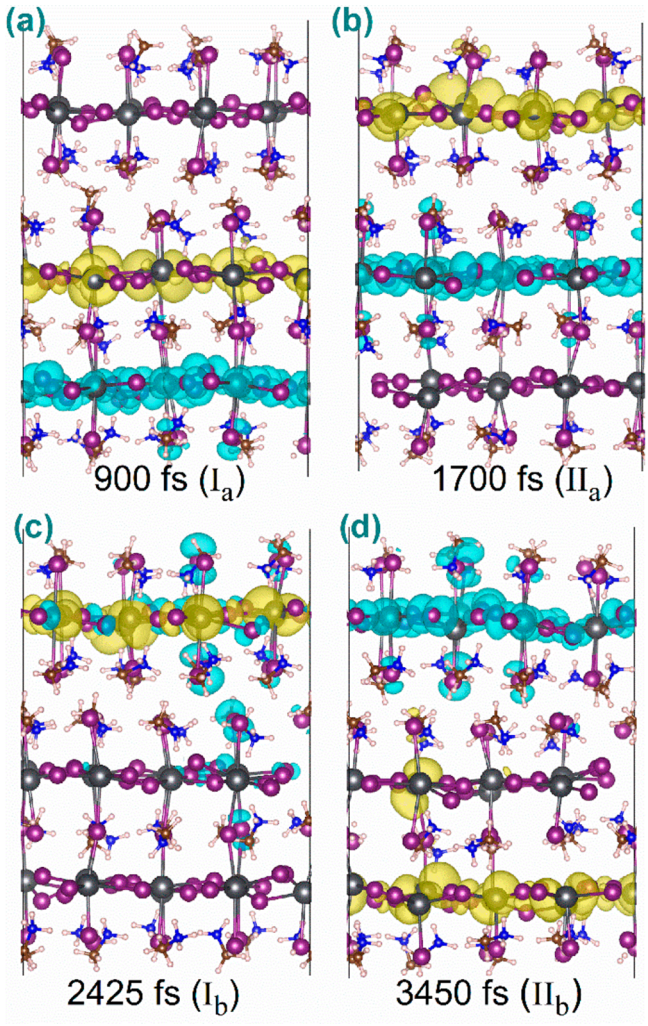

Figure 3. Charge density of the lowest-energy exciton at selected snapshots of $MA_2PbI_4/MA_3Pb_2I_7$ heterostructure, (a) 900 fs, (b) 1700 fs, (c) 2425 fs, and (d) 3450 fs, during the BOMD simulation. The electron and hole density is shown in yellow and cyan, respectively.

remain the same (see Figure S5 and S6). Thus, we believe that the coexistence of both types of band alignment can also happen in a thicker heterostructure at room temperature.

To correlate the structural deformation with the shifts in the band structure, we perform the Fourier transform (FT) for the CBM and the VBM from the time domain (Figure 2a) to the frequency domain (Figure 2c). The intensity of the FT spectrum represents the strength of electron−phonon coupling in the heterostructure. It is found that the phonon modes below 200 cm^{-1} dominate the FT spectra for both the CBM and VBM, and they stem from the atomic vibrations in the inorganic lead−iodide layers (e.g., Pb−I stretching modes, etc.)[S7−S9] The spectral intensity of the VBM is generally stronger than that of the CBM, implying a greater fluctuation of the VBM than the CBM, consistent with results shown in Figure 2a. We have also examined the time evolution of Pb−I−Pb bond angles in the $MA_2PbI_4/MA_3Pb_2I_7$ heterostructure and found significant changes of the angles, from ∼120° to ∼165° (Figure S7). The results confirm the "softness" of the inorganic layers of the perovskites.

To place the above results on a more general ground, we consider two additional heterostructures by replacing the MA

https://dx.doi.org/10.1021/acs.jpclett.0c00376
J. Phys. Chem. Lett. 2020, 11, 2910−2916

cation in $MA_2PbI_4/MA_3Pb_2I_7$ with BA and PDA cations as spacers. The chemical formula of the two new heterostructures is $BA_2PbI_4/BA_2MAPb_2I_7$ and $BA(PDA)_{0.5}PbI_4/BA(PDA)_{0.5}MAPb_2I_7$, respectively. Note that both BA and PDA cations have been used experimentally as spacers in 2D heterostructures.[60−62] BA cations are introduced at the top/bottom surface layers of the $BA(PDA)_{0.5}PbI_4/BA(PDA)_{0.5}MAPb_2I_7$ heterostructure to maintain charge neutrality. The atomic structures of the heterojunctions can be found in Figure S8. The $BA_2PbI_4/BA_2MAPb_2I_7$ heterostructure, which is still in the RP phase, consists of a monolayer BA_2PbI_4 (n = 1) and a monolayer $BA_2MAPb_2I_7$ (n = 2). By contrast, the $BA(PDA)_{0.5}PbI_4/BA(PDA)_{0.5}MAPb_2I_7$ heterostructure, which belongs to the DJ phase, consists of a monolayer $BA(PDA)_{0.5}PbI_4$ (n = 1) and a monolayer $BA(PDA)_{0.5}MAPb_2I_7$ (n = 2).

Similarly, we calculate the band structure of the two heterostructures using the DFT-RSH method and results are displayed in Figure 4a,b. In contrast to the $MA_2PbI_4/MA_3Pb_2I_7$ heterostructure, the new heterostructures both exhibit the type-I band alignment at 0 K. In other words, interfacial energy as opposed to charge transfer should take place in the two heterostructures. The conduction and valence band offset for the $BA_2PbI_4/BA_2MAPb_2I_7$ heterostructure is 0.24 and 0.19 eV, respectively, while the conduction and valence offset for the $BA(PDA)_{0.5}PbI_4/BA(PDA)_{0.5}MAPb_2I_7$ heterostructure is 0.18 and 0.15 eV, respectively. To examine the effect of thermal fluctuations on the band alignment, we perform the BOMD simulations at 300 K for the two heterostructures. As shown in Figure 4c, we find that the energy fluctuation in the CBM and VBM of $BA_2PbI_4/BA_2MAPb_2I_7$ heterostructure is about 0.43 and 0.59 eV, respectively. Similarly, the energy fluctuation in the CBM and VBM of the $BA(PDA)_{0.5}PbI_4/BA(PDA)_{0.5}MAPb_2I_7$ heterostructure is 0.37 and 0.54 eV, respectively, shown in Figure 4d. Apparently, the energy fluctuations of the CBM and VBM in both heterostructures at 300 K are greater than the band offsets at 0 K, suggesting that both types of band alignments can arise simultaneously in the heterostructures, driven by thermal fluctuations. The charge density distributions of the lowest-energy exciton at selected snapshots are shown in Figure S9 and S10, supporting the fact that both the type-I and type-II band alignments can be formed in the heterostructures at 300 K. Therefore, we have shown that the 2D perovskite heterostructures are in general prone to the coexistence of both types of band alignment. The fact that the band alignment at room temperature differs from that at zero temperature, i.e., band "misalignment", suggests that the electron−phonon coupling in the 2D heterostructures is so strong that it cannot be ignored in designing 2D heterostructures.

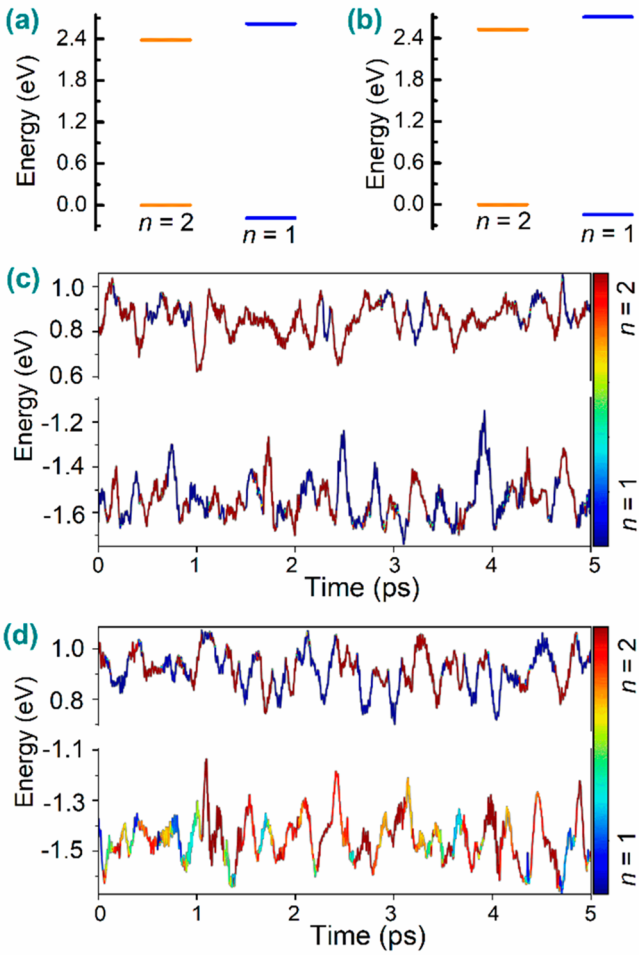

Figure 4. Band alignment of (a) $BA_2PbI_4/BA_2MAPb_2I_7$ and (b) $BA(PDA)_{0.5}PbI_4/BA(PDA)_{0.5}MAPb_2I_7$ heterostructures at 0 K. The VBM of each heterostructure is set to zero. The time evolution of the VBM and CBM in (c) $BA_2PbI_4/BA_2MAPb_2I_7$ and (d) $BA(PDA)_{0.5}PbI_4/BA(PDA)_{0.5}MAPb_2I_7$ heterostructures during the BOMD simulation.

For applications of 2D perovskite heterostructures, a robust band alignment is a must. For example, in photovoltaic applications, the heterostructure has to maintain the type-II band alignment for efficient charge separation throughout the operation time scale. Similarly, in light-emitting applications, the heterostructure has to preserve the type-I band alignment for efficient energy transfer. Any deviation or disruption of the band alignment is detrimental to the intended applications. Our calculations suggest that there are two ways to stabilize the band alignment of a 2D heterostructure at room temperature; one can try to decrease the electron−phonon coupling or to increase the band offsets. Here, we attempt to increase the band offsets of the heterostructures. Because the band alignment is determined primarily by the inorganic layers of 2D perovskites, we seek to modify the inorganic layers in one of the two perovskites while keeping the other intact. More specifically, we replace I^- ions in MA_2PbI_4 by Br^- ions, and the new heterostructure (Figure 5a) consists of a monolayer MA_2PbBr_4 (n = 1) and a monolayer $MA_3Pb_2I_7$ (n = 2). As shown in Figure 5b, the type-II band alignment is formed in the engineered heterostructure at 0 K, with a much increased valence band offset of 0.78 eV (the conduction band offset is 0.24 eV). In addition, the TDDFT calculations clearly show charge separation (Figure 5a), confirming the type-II band alignment at 0 K.

We then perform the BOMD simulations to examine thermal fluctuation of the band structure at 300 K. As shown in Figure 5c, the energy fluctuation in the CBM and VBM reaches 0.56 and 0.44 eV, respectively. The energy fluctuation in the CBM at 300 K is greater than the conduction band offset at 0 K, and as a result, the CBM switches between the perovskites (from n = 1 to n = 2) during the BOMD simulation (Figure 5c). In contrast, the energy fluctuation in the VBM is smaller than the valence band offset at 0 K, and thus no switching (from n = 2 to n = 1) is observed in Figure 5c. We

https://dx.doi.org/10.1021/acs.jpclett.0c00376
J. Phys. Chem. Lett. 2020, 11, 2910−2916

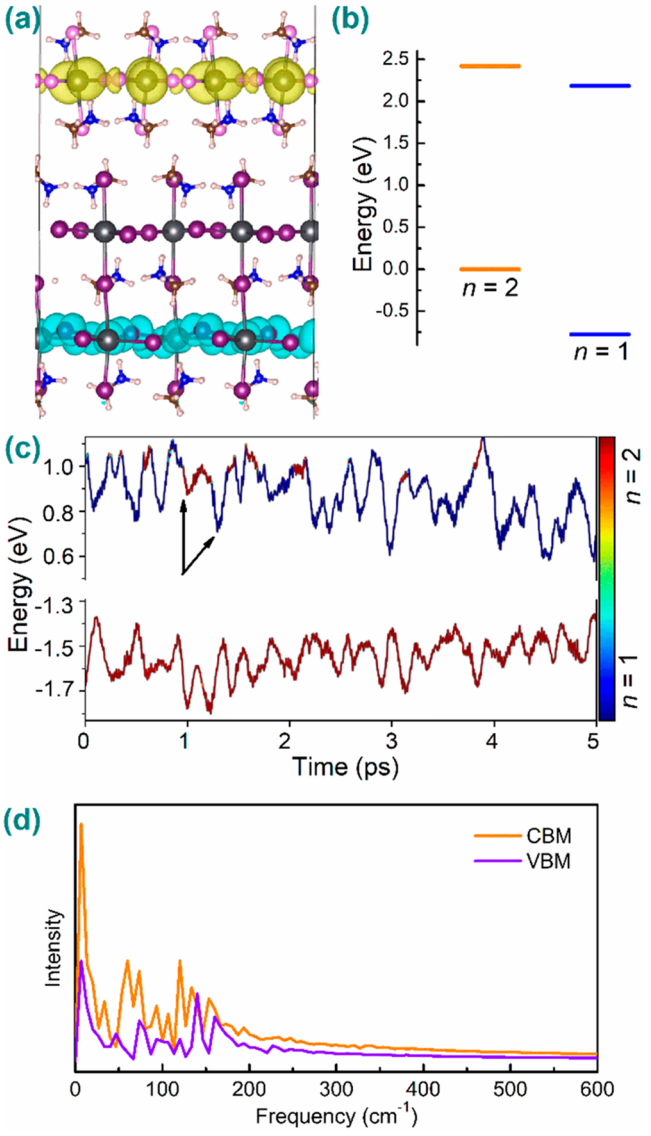

Figure 5. (a) Atomic structure and exciton charge density of $MA_2PbBr_4/MA_3Pb_2I_7$ heterostructure. Br atoms are represented by pink spheres, and the electron and hole densities are shown in yellow and cyan, respectively. (b) Band alignment of $MA_2PbBr_4/MA_3Pb_2I_7$ heterostructure at 0 K. The VBM of the heterostructure is set to zero. (c) Time evolution of the VBM and CBM of $MA_2PbBr_4/MA_3Pb_2I_7$ heterostructure during the BOMD simulation. The black arrows indicate the switch of band alignment. (d) Fourier transform of (c) from the time domain to the frequency domain.

have also calculated the percentage of the two types of band alignment during the BOMD simulation for $MA_2PbBr_4/MA_3Pb_2I_7$ heterostructure, and the percentage of the type-I band alignment in the modified heterostructure is found to reduce significantly compared to the original heterostructure (Table 1). Moreover, only two energy alignments (I_a and II_a) can be formed in the modified heterostructure, in contrast to four different alignments in the original heterostructure. Therefore, increasing band offsets by tuning the inorganic layers appears to be an effective means of suppressing band misalignment of the 2D heterostructures. Finally, we perform the FT for CBM and VBM from the time domain (Figure 5c) to the frequency domain (Figure 5d). Similar to $MA_2PbI_4/MA_3Pb_2I_7$ heterostructure, the phonon modes below 200 cm^{-1} dominate the FT spectra for both CBM and VBM. However, the spectral intensity of CBM is stronger than that of VBM, implying a greater energy fluctuation of CBM.

To summarize, we propose that the 2D perovskite heterostructures are prone to band "misalignment" induced by thermal fluctuations, which explains the contradictory experimental observations on the band alignments. By means of first-principles calculations, we have shown that both the type-I and type-II band alignments could coexist in typical 2D perovskite heterostructures, such as $MA_2PbI_4/MA_3Pb_2I_7$, $BA_2PbI_4/BA_2MAPb_2I_7$, and $BA(PDA)_{0.5}PbI_4/BA(PDA)_{0.5}MAPb_2I_7$, owing to the "softness" of the inorganic layers and strong electron−phonon coupling at room temperature. We further demonstrate that by tuning the inorganic layers of the 2D perovskites, one can increase the band offsets and suppress the band "misalignment" of 2D perovskite heterostructures so as to maintain robust band alignments at room temperature.

■ ASSOCIATED CONTENT

Supporting Information

The Supporting Information is available free of charge at https://pubs.acs.org/doi/10.1021/acs.jpclett.0c00376.

Computational details, figures of band alignments, structures, time evolution graphs, and charge distributions, and a table of energy difference (PDF)

■ AUTHOR INFORMATION

Corresponding Author

Gang Lu − *Department of Physics and Astronomy, California State University, Northridge, Northridge, California 91330-8268, United States;* orcid.org/0000-0002-9168-8968; Email: ganglu@csun.edu

Authors

Linghai Zhang − *Department of Physics and Astronomy, California State University, Northridge, Northridge, California 91330-8268, United States;* orcid.org/0000-0003-0536-5765

Xu Zhang − *Department of Physics and Astronomy, California State University, Northridge, Northridge, California 91330-8268, United States;* orcid.org/0000-0002-6491-3234

Complete contact information is available at: https://pubs.acs.org/10.1021/acs.jpclett.0c00376

Notes

The authors declare no competing financial interest.

■ ACKNOWLEDGMENTS

The work was supported by the U.S. National Science Foundation (DMR1828019) and the U.S. Army Research Office (W911NF1810473).

■ REFERENCES

(1) Stoumpos, C. C.; Kanatzidis, M. G. The Renaissance of Halide Perovskites and Their Evolution as Emerging Semiconductors. *Acc. Chem. Res.* **2015**, *48*, 2791−2802.

(2) Manser, J. S.; Christians, J. A.; Kamat, P. V. Intriguing Optoelectronic Properties of Metal Halide Perovskites. *Chem. Rev.* **2016**, *116*, 12956−13008.

(3) Snaith, H. J. Present Status and Future Prospects of Perovskite Photovoltaics. *Nat. Mater.* **2018**, *17*, 372−376.

(4) Fu, Y.; Zhu, H.; Schrader, A. W.; Liang, D.; Ding, Q.; Joshi, P.; Hwang, L.; Zhu, X. Y.; Jin, S. Nanowire Lasers of Formamidinium Lead Halide Perovskites and Their Stabilized Alloys with Improved Stability. *Nano Lett.* **2016**, *16*, 1000−1008.
(5) Mai, R.; Wu, X.; Jiang, Y.; Meng, Y.; Liu, B.; Hu, X.; Roncali, J.; Zhou, G.; Liu, J.-M.; Kempa, K.; et al. An Efficient Multi-Functional Material Based on Polyether-Substituted Indolocarbazole for Perovskite Solar Cells and Solution-Processed Non-Doped OLEDs. *J. Mater. Chem. A* **2019**, *7*, 1539−1547.
(6) Huang, H.; Bodnarchuk, M. I.; Kershaw, S. V.; Kovalenko, M. V.; Rogach, A. L. Lead Halide Perovskite Nanocrystals in the Research Spotlight: Stability and Defect Tolerance. *ACS Energy Lett.* **2017**, *2*, 2071−2083.
(7) Tong, C.-J.; Li, L.; Liu, L.-M.; Prezhdo, O. V. Long Carrier Lifetimes in PbI_2-Rich Perovskites Rationalized by Ab Initio Nonadiabatic Molecular Dynamics. *ACS Energy Lett.* **2018**, *3*, 1868−1874.
(8) Wei, L.-y.; Ma, W.; Lian, C.; Meng, S. Benign Interfacial Iodine Vacancies in Perovskite Solar Cells. *J. Phys. Chem. C* **2017**, *121*, 5905−5913.
(9) Lee, D.-K.; Jeong, D.-N.; Ahn, T. K.; Park, N.-G. Precursor Engineering for a Large-Area Perovskite Solar Cell with > 19% Efficiency. *ACS Energy Lett.* **2019**, *4*, 2393−2401.
(10) Yum, J.-H.; Moon, S.-J.; Yao, L.; Caretti, M.; Nicolay, S.; Kim, D.-H.; Sivula, K. Robust Electron Transport Layers via In Situ Cross-Linking of Perylene Diimide and Fullerene for Perovskite Solar Cells. *ACS Appl. Energy Mater.* **2019**, *2*, 6616−6623.
(11) Lindblad, R.; Jena, N. K.; Philippe, B.; Oscarsson, J.; Bi, D.; Lindblad, A.; Mandal, S.; Pal, B.; Sarma, D. D.; Karis, O.; et al. Electronic Structure of $CH_3NH_3PbX_3$ Perovskites: Dependence on the Halide Moiety. *J. Phys. Chem. C* **2015**, *119*, 1818−1825.
(12) Grancini, G.; Roldán-Carmona, C.; Zimmermann, I.; Mosconi, E.; Lee, X.; Martineau, D.; Narbey, S.; Oswald, F.; De Angelis, F.; Graetzel, M.; et al. One-Year Stable Perovskite Solar Cells by 2D/3D Interface Engineering. *Nat. Commun.* **2017**, *8*, 15684.
(13) Wygant, B. R.; Ye, A. Z.; Dolocan, A.; Vu, Q.; Abbot, D. M.; Mullins, C. B. Probing the Degradation Chemistry and Enhanced Stability of 2D Organolead Halide Perovskites. *J. Am. Chem. Soc.* **2019**, *141*, 18170−18181.
(14) Yang, Y.; Gao, F.; Gao, S.; Wei, S.-H. Origin of the Stability of Two-Dimensional Perovskites: A First-Principles Study. *J. Mater. Chem. A* **2018**, *6*, 14949−14955.
(15) Diau, E. W.-G.; Jokar, E.; Rameez, M. Strategies To Improve Performance and Stability for Tin-Based Perovskite Solar Cells. *ACS Energy Lett.* **2019**, *4*, 1930−1937.
(16) Huang, P.; Kazim, S.; Wang, M.; Ahmad, S. Toward Phase Stability: Dion−Jacobson Layered Perovskite for Solar Cells. *ACS Energy Lett.* **2019**, *4*, 2960−2974.
(17) Zheng, Y.; Niu, T.; Ran, X.; Qiu, J.; Li, B.; Xia, Y.; Chen, Y.; Huang, W. Unique Characteristics of 2D Ruddlesden−Popper (2DRP) Perovskite for Future Photovoltaic Application. *J. Mater. Chem. A* **2019**, *7*, 13860−13872.
(18) Nan, G.; Zhang, X.; Lu, G. Self-Healing of Photocurrent Degradation in Perovskite Solar Cells: The Role of Defect-Trapped Excitons. *J. Phys. Chem. Lett.* **2019**, *10*, 7774−7780.
(19) Saliba, M.; Bakr, O. M.; Pradhan, N.; Kuno, M.; Kamat, P. V. Energy Spotlight: New Inroads in Metal Halide Perovskite Research. *ACS Energy Lett.* **2019**, *4*, 3036−3038.
(20) Fan, W.; Shi, Y.; Shi, T.; Chu, S.; Chen, W.; Ighodalo, K. O.; Zhao, J.; Li, X.; Xiao, Z. Suppression and Reversion of Light-Induced Phase Separation in Mixed-Halide Perovskites by Oxygen Passivation. *ACS Energy Lett.* **2019**, *4*, 2052−2058.
(21) Frost, J. M.; Butler, K. T.; Brivio, F.; Hendon, C. H.; van Schilfgaarde, M.; Walsh, A. Atomistic Origins of High-Performance in Hybrid Halide Perovskite Solar Cells. *Nano Lett.* **2014**, *14*, 2584−2590.
(22) Smith, I. C.; Hoke, E. T.; Solis-Ibarra, D.; McGehee, M. D.; Karunadasa, H. I. A Layered Hybrid Perovskite Solar-Cell Absorber with Enhanced Moisture Stability. *Angew. Chem., Int. Ed.* **2014**, *53*, 11232−11235.
(23) Stoumpos, C. C.; Cao, D. H.; Clark, D. J.; Young, J.; Rondinelli, J. M.; Jang, J. I.; Hupp, J. T.; Kanatzidis, M. G. Ruddlesden−Popper Hybrid Lead Iodide Perovskite 2D Homologous Semiconductors. *Chem. Mater.* **2016**, *28*, 2852−2867.
(24) Mao, L.; Ke, W.; Pedesseau, L.; Wu, Y.; Katan, C.; Even, J.; Wasielewski, M. R.; Stoumpos, C. C.; Kanatzidis, M. G. Hybrid Dion−Jacobson 2D Lead Iodide Perovskites. *J. Am. Chem. Soc.* **2018**, *140*, 3775−3783.
(25) Li, T.; Chen, X.; Wang, X.; Lu, H.; Yan, Y.; Beard, M. C.; Mitzi, D. B. Origin of Broad-Band Emission and Impact of Structural Dimensionality in Tin-Alloyed Ruddlesden−Popper Hybrid Lead Iodide Perovskites. *ACS Energy Lett.* **2020**, *5*, 347−352.
(26) Wang, D.; Wen, B.; Zhu, Y.-N.; Tong, C.-J.; Tang, Z.-K.; Liu, L.-M. First-Principles Study of Novel Two-Dimensional $(C_4H_9NH_3)_2PbX_4$ Perovskites for Solar Cell Absorbers. *J. Phys. Chem. Lett.* **2017**, *8*, 876−883.
(27) Zhang, S.-F.; Chen, X.-K.; Ren, A.-M.; Li, H.; Bredas, J.-L. Impact of Organic Spacers on the Carrier Dynamics in 2D Hybrid Lead-Halide Perovskites. *ACS Energy Lett.* **2019**, *4*, 17−25.
(28) Zhang, Z.; Fang, W.-H.; Long, R.; Prezhdo, O. V. Exciton Dissociation and Suppressed Charge Recombination at 2D Perovskite Edges: Key Roles of Unsaturated Halide Bonds and Thermal Disorder. *J. Am. Chem. Soc.* **2019**, *141*, 15557−15566.
(29) Zhu, X.; Xu, Z.; Zuo, S.; Feng, J.; Wang, Z.; Zhang, X.; Zhao, K.; Zhang, J.; Liu, H.; Priya, S.; et al. Vapor-Fumigation for Record Efficiency Two-Dimensional Perovskite Solar Cells with Superior Stability. *Energy Environ. Sci.* **2018**, *11*, 3349−3357.
(30) Ahmad, S.; Fu, P.; Yu, S.; Yang, Q.; Liu, X.; Wang, X.; Wang, X.; Guo, X.; Li, C. Dion-Jacobson Phase 2D Layered Perovskites for Solar Cells with Ultrahigh Stability. *Joule* **2019**, *3*, 794−806.
(31) Leng, K.; Abdelwahab, I.; Verzhbitskiy, I.; Telychko, M.; Chu, L.; Fu, W.; Chi, X.; Guo, N.; Chen, Z.; Chen, Z.; et al. Molecularly Thin Two-Dimensional Hybrid Perovskites with Tunable Optoelectronic Properties due to Reversible Surface Relaxation. *Nat. Mater.* **2018**, *17*, 908−914.
(32) Mao, L.; Teicher, S. M. L.; Stoumpos, C. C.; Kennard, R. M.; DeCrescent, R. A.; Wu, G.; Schuller, J. A.; Chabinyc, M. L.; Cheetham, A. K.; Seshadri, R. Chemical and Structural Diversity of Hybrid Layered Double Perovskite Halides. *J. Am. Chem. Soc.* **2019**, *141*, 19099−19109.
(33) Smith, M. D.; Crace, E. J.; Jaffe, A.; Karunadasa, H. I. The Diversity of Layered Halide Perovskites. *Annu. Rev. Mater. Res.* **2018**, *48*, 111−136.
(34) Ding, Y.-F.; Zhao, Q.-Q.; Yu, Z.-L.; Zhao, Y.-Q.; Liu, B.; He, P.-B.; Zhou, H.; Li, K.; Yin, S.-F.; Cai, M.-Q. Strong Thickness-Dependent Quantum Confinement in All-Inorganic Perovskite Cs_2PbI_4 with A Ruddlesden−Popper Structure. *J. Mater. Chem. C* **2019**, *7*, 7433−7441.
(35) Zhao, Y.-Q.; Ma, Q.-R.; Liu, B.; Yu, Z.-L.; Yang, J.; Cai, M.-Q. Layer-Dependent Transport and Optoelectronic Property in Two-Dimensional Perovskite: $(PEA)_2PbI_4$. *Nanoscale* **2018**, *10*, 8677−8688.
(36) Pan, L.-Y.; Ding, Y.-F.; Yu, Z.-L.; Wan, Q.; Liu, B.; Cai, M.-Q. Layer-Dependent Optoelectronic Property for All-Inorganic Two-Dimensional Mixed Halide Perovskite $Cs_2PbI_2Cl_2$ with A Ruddlesden-Popper Structure. *J. Power Sources* **2020**, *451*, 227732.
(37) Qing, J.; Liu, X.-K.; Li, M.; Liu, F.; Yuan, Z.; Tiukalova, E.; Yan, Z.; Duchamp, M.; Chen, S.; Wang, Y.; et al. Aligned and Graded Type-II Ruddlesden−Popper Perovskite Films for Efficient Solar Cells. *Adv. Energy Mater.* **2018**, *8*, 1800185.
(38) Yuan, M.; Quan, L. N.; Comin, R.; Walters, G.; Sabatini, R.; Voznyy, O.; Hoogland, S.; Zhao, Y.; Beauregard, E. M.; Kanjanaboos, P.; et al. Perovskite Energy Funnels for Efficient Light-Emitting Diodes. *Nat. Nanotechnol.* **2016**, *11*, 872−877.
(39) Hwang, B.; Lee, J.-S. 2D Perovskite-Based Self-Aligned Lateral Heterostructure Photodetectors Utilizing Vapor Deposition. *Adv. Opt. Mater.* **2019**, *7*, 1801356.

https://dx.doi.org/10.1021/acs.jpclett.0c00376
J. Phys. Chem. Lett. 2020, 11, 2910−2916

(40) Wei, K.; Jiang, T.; Xu, Z.; Zhou, J.; You, J.; Tang, Y.; Li, H.; Chen, R.; Zheng, X.; Wang, S.; et al. Ultrafast Carrier Transfer Promoted by Interlayer Coulomb Coupling in 2D/3D Perovskite Heterostructures. *Laser Photonics Rev.* **2018**, *12*, 1800128.
(41) Zheng, K.; Chen, Y.; Sun, Y.; Chen, J.; Chábera, P.; Schaller, R.; Al-Marri, M. J.; Canton, S. E.; Liang, Z.; Pullerits, T. Inter-Phase Charge and Energy Transfer in Ruddlesden−Popper 2D Perovskites: Critical Role of the Spacing Cations. *J. Mater. Chem. A* **2018**, *6*, 6244−6250.
(42) Liu, J.; Leng, J.; Wu, K.; Zhang, J.; Jin, S. Observation of Internal Photoinduced Electron and Hole Separation in Hybrid Two-Dimentional Perovskite Films. *J. Am. Chem. Soc.* **2017**, *139*, 1432−1435.
(43) Williams, O. F.; Guo, Z.; Hu, J.; Yan, L.; You, W.; Moran, A. M. Energy Transfer Mechanisms in Layered 2D Perovskites. *J. Chem. Phys.* **2018**, *148*, 134706.
(44) Fu, Y.; Zheng, W.; Wang, X.; Hautzinger, M. P.; Pan, D.; Dang, L.; Wright, J. C.; Pan, A.; Jin, S. Multicolor Heterostructures of Two-Dimensional Layered Halide Perovskites that Show Interlayer Energy Transfer. *J. Am. Chem. Soc.* **2018**, *140*, 15675−15683.
(45) Shang, Q.; Wang, Y.; Zhong, Y.; Mi, Y.; Qin, L.; Zhao, Y.; Qiu, X.; Liu, X.; Zhang, Q. Unveiling Structurally Engineered Carrier Dynamics in Hybrid Quasi-Two-Dimensional Perovskite Thin Films toward Controllable Emission. *J. Phys. Chem. Lett.* **2017**, *8*, 4431−4438.
(46) Wang, J.; Mi, Y.; Gao, X.; Li, J.; Li, J.; Lan, S.; Fang, C.; Shen, H.; Wen, X.; Chen, R.; et al. Giant Nonlinear Optical Response in 2D Perovskite Heterostructures. *Adv. Opt. Mater.* **2019**, *7*, 1900398.
(47) Mahata, A.; Mosconi, E.; Meggiolaro, D.; De Angelis, F. Modulating Band Alignment in Mixed Dimensionality 3D/2D Perovskites by Surface Termination Ligand Engineering. *Chem. Mater.* **2020**, *32*, 105−113.
(48) Meggiolaro, D.; Mosconi, E.; Proppe, A. H.; Quintero-Bermudez, R.; Kelley, S. O.; Sargent, E. H.; De Angelis, F. Energy Level Tuning at the $MAPbI_3$ Perovskite/Contact Interface Using Chemical Treatment. *ACS Energy Lett.* **2019**, *4*, 2181−2184.
(49) Quintero-Bermudez, R.; Proppe, A. H.; Mahata, A.; Todorović, P.; Kelley, S. O.; De Angelis, F.; Sargent, E. H. Ligand-Induced Surface Charge Density Modulation Generates Local Type-II Band Alignment in Reduced-Dimensional Perovskites. *J. Am. Chem. Soc.* **2019**, *141*, 13459−13467.
(50) Leininger, T.; Stoll, H.; Werner, H.-J.; Savin, A. Combining Long-Range Configuration Interaction with Short-Range Density Functionals. *Chem. Phys. Lett.* **1997**, *275*, 151−160.
(51) Iikura, H.; Tsuneda, T.; Yanai, T.; Hirao, K. A Long-Range Correction Scheme for Generalized-Gradient-Approximation Exchange Functionals. *J. Chem. Phys.* **2001**, *115*, 3540−3544.
(52) Tawada, Y.; Tsuneda, T.; Yanagisawa, S.; Yanai, T.; Hirao, K. A Long-Range-Corrected Time-Dependent Density Functional Theory. *J. Chem. Phys.* **2004**, *120*, 8425−8433.
(53) Blancon, J. C.; Stier, A. V.; Tsai, H.; Nie, W.; Stoumpos, C. C.; Traoré, B.; Pedesseau, L.; Kepenekian, M.; Katsutani, F.; Noe, G. T.; et al. Scaling Law for Excitons in 2D Perovskite Quantum Wells. *Nat. Commun.* **2018**, *9*, 2254.
(54) Molina-Sánchez, A. Excitonic States in Semiconducting Two-Dimensional Perovskites. *ACS Appl. Energy Mater.* **2018**, *1*, 6361−6367.
(55) Yaffe, O.; Chernikov, A.; Norman, Z. M.; Zhong, Y.; Velauthapillai, A.; van der Zande, A.; Owen, J. S.; Heinz, T. F. Excitons in Ultrathin Organic-Inorganic Perovskite Crystals. *Phys. Rev. B: Condens. Matter Mater. Phys.* **2015**, *92*, 045414.
(56) Gao, Y.; Zhang, M.; Zhang, X.; Lu, G. Decreasing Exciton Binding Energy in Two-Dimensional Halide Perovskites by Lead Vacancies. *J. Phys. Chem. Lett.* **2019**, *10*, 3820−3827.
(57) Thouin, F.; Valverde-Chávez, D. A.; Quarti, C.; Cortecchia, D.; Bargigia, I.; Beljonne, D.; Petrozza, A.; Silva, C.; Srimath Kandada, A. R. Phonon Coherences Reveal the Polaronic Character of Excitons in Two-Dimensional Lead Halide Perovskites. *Nat. Mater.* **2019**, *18*, 349−356.
(58) Cortecchia, D.; Neutzner, S.; Srimath Kandada, A. R.; Mosconi, E.; Meggiolaro, D.; De Angelis, F.; Soci, C.; Petrozza, A. Broadband Emission in Two-Dimensional Hybrid Perovskites: The Role of Structural Deformation. *J. Am. Chem. Soc.* **2017**, *139*, 39−42.
(59) Quarti, C.; Grancini, G.; Mosconi, E.; Bruno, P.; Ball, J. M.; Lee, M. M.; Snaith, H. J.; Petrozza, A.; De Angelis, F. The Raman Spectrum of the $CH_3NH_3PbI_3$ Hybrid Perovskite: Interplay of Theory and Experiment. *J. Phys. Chem. Lett.* **2014**, *5*, 279−284.
(60) Zheng, Y.; Niu, T.; Qiu, J.; Chao, L.; Li, B.; Yang, Y.; Li, Q.; Lin, C.; Gao, X.; Zhang, C.; et al. Oriented and Uniform Distribution of Dion−Jacobson Phase Perovskites Controlled by Quantum Well Barrier Thickness. *Solar RRL* **2019**, *3*, 1900090.
(61) Sheikh, T.; Shinde, A.; Mahamuni, S.; Nag, A. Possible Dual Bandgap in $(C_4H_9NH_3)_2PbI_4$ 2D Layered Perovskite: Single-Crystal and Exfoliated Few-Layer. *ACS Energy Lett.* **2018**, *3*, 2940−2946.
(62) Liao, J.-F.; Rao, H.-S.; Chen, B.-X.; Kuang, D.-B.; Su, C.-Y. Dimension Engineering on Cesium Lead Iodide for Efficient and Stable Perovskite Solar Cells. *J. Mater. Chem. A* **2017**, *5*, 2066−2072.

https://dx.doi.org/10.1021/acs.jpclett.0c00376
J. Phys. Chem. Lett. 2020, 11, 2910−2916